applied sciences

MDPI

Article

Dielectric and Impedance Analysis on the Electrical Response of Lead-Free $Ba_{1-x}Ca_xTi_{0.9}Zr_{0.1}O_3$ Ceramics at High Temperature Range

Armando Reyes-Montero [1], Paola Ramos-Alvarez [1], Amador M. González [2], Rigoberto López-Juárez [3] and María Elena Villafuerte-Castrejón [1,*]

1 Instituto de Investigaciones en Materiales, Universidad Nacional Autónoma de México, Circuito Exterior S/N, A.P. 70-360 CDMX, Mexico; ingaremo@gmail.com (A.R.-M.); paolaeramosalvarez@gmail.com (P.R.-A.)

2 Grupo POEMMA, ETSIS Telecomunicación, Campus Sur, Universidad Politécnica de Madrid, Ctra. Valencia Km 7, 28031 Madrid, Spain; amador@etsist.upm.es

3 Unidad Morelia del Instituto de Investigaciones en Materiales, Universidad Nacional Autónoma de México, Antigua Carretera a Pátzcuaro No. 8701, Col. Ex Hacienda de San José de la Huerta, C.P. 58190 Morelia, Mexico; rlopez@iim.unam.mx

* Correspondence: mevc@unam.mx; Tel.: +52-55-5622-4646

Academic Editors: José Francisco Fernández and Fernando Rubio-Marcos
Received: 22 December 2016; Accepted: 14 February 2017; Published: 23 February 2017

Abstract: $Ba_{1-x}Ca_xTi_{0.9}Zr_{0.1}O_3$ (x = 0.10, 0.15, 0.18) solid solutions were synthesized by the conventional solid-state method. A perovskite-type structure was determined using the X-ray diffraction (XRD) technique. The addition of Ca^{2+} reduced the grain size (22.6, 17.9 and 13.3 μm, respectively) for all well-sintered ceramics (≈98%). Moreover, the stability temperature ranges for the tetragonal phase were promoted by displacing the ferroelectric-ferroelectric phase's transition temperatures while T_C was maintained (86 °C). The electrical performance of the material improved as the stoichiometric composition was positioned near the morphotropic phase boundary (x = 0.15): $\varepsilon_r \approx 16{,}500$ (T_C) at 1 kHz. For $T > T_C$, a thermally activated relaxation process occurred. In addition, the bulk and grain boundary processes were responsible for the conduction mechanisms. The composition x = 0.15 showed an activation energy of Ea = 1.49 eV with a maximum conductivity of $\sigma_{max} = 2.48 \times 10^{-2}$ S·cm^{-1} at 580 °C. Systematic studies at high temperature for dielectric properties were accomplished for analyzing electrical inhomogeneities associated with the grain, grain boundaries or surfaces, which are important for device design and a fundamental electrical characterization.

Keywords: BCTZ ceramics; dielectric response; impedance spectroscopy

1. Introduction

Due to their optimum dielectric, piezoelectric and ferroelectric response, lead-free based electroceramics have been proposed as an alternative to $Pb(Zr_{1-x}Ti_x)O_3$ (PZT). In particular, $Ba_{1-x}Ca_xT_{1-y}Zr_yO_3$ (BCTZ) solid solution shows a phase diagram similar to PZT systems with a morphotropic phase boundary (MPB) responsible for its high electrical performance. The coalescence of two ferroelectric phases lowers down the energy barrier between them, facilitating the rotation grade of the polarization vector [1]. For this reason, several researchers have focused their attention on modifying the chemical composition [2–5] or synthesis conditions [6–8] for maximizing their electrical properties.

For high-temperature conditions ($T > T_C$), a systematic study of the electrical behavior for BCTZ has not been presented. Moreover, the influence that Ca^{2+} doping has over dielectric conditions

and the associated conduction mechanism has not fully been explained. In order to investigate ceramic relaxation phenomena and structural features related to conduction mechanisms, impedance spectroscopy (IS) arises as an efficient technique [9].

The dielectric process, in polycrystalline materials, involves the movement of electric carriers. Therefore, it is important to separate between the different responsible microstructural regions. To characterize the microstructure of the material, IS measurements are made over a wide range of frequencies to distinguish between different regions [10–12]: grains, grain boundary, sample/electrode interface, etc. Using a variable-frequency measurement, regardless the nature of the material under study, the analysis of the alternating current (AC) data requires considerable care in order to (a) assign the different electrical impedances to the appropriate regions of the sample and (b) extract the maximum amount of useful information from the data available [13]. This is how experimental information obtained is represented by appropriate equivalent circuits, useful for determining component resistance and capacitance parameters.

In the present work the influence of Ca^{2+} on the structure and phase transition behavior was studied. The effect of the microstructure on the dielectric and conduction characteristics was analyzed. Finally, the dielectric relaxation and activation energy was calculated for thermally activated electrical processes.

2. Materials and Methods

$Ba_{1-x}Ca_xTi_{0.9}Zr_{0.1}O_3$ solid solutions (x = 0.10, 0.15, 0.18) were prepared by conventional solid state method. $BaCO_3$ (99.0%, Analytyca, Monterrey, Mexico), $CaCO_3$ (99.0%, Fluka, Seelze, Germany), TiO_2 (99.0%, Aldrich, St. Louis, MO, USA) and ZrO_2 (99.0%, Riedel-deHaën, Seelze, Germany) were used as starting materials. Reagents were dried at 200 °C for 2 h, weighted according to the stoichiometry ratio and mixed for 30 min in an agate mortar using acetone. Afterwards, the mixture was calcined at 1250 °C for 2 h, followed by a ball-milling process (product ground by zirconia balls using ethanol as grinding media for 24 h). Finally, powders were uniaxially pressed into pellets (~13.0 mm diameter; ~1.5 mm thickness, 40 MPa) and sintered at 1400 °C for 2 h in air.

Phase structure of BCTZ ceramics was identified using X-ray diffraction (D-8 Advance, Bruker Co., Billerica, MA, USA) with Cu Kα radiation, 0.016° step size (2θ) and 1 s of integration time. The microstructure of samples was analyzed by field emission scanning electron microscope (JSM-7600F, JEOL, Peabody, MA, USA). The EDS spectra were recorded with an INCA X-ray microanalysis system (EDX, Oxford Instruments plc., Oxfordshire, UK). Average grain size of a large sample area was determined using a computer-aided image analysis (ImageJ software, National Institutes of Health (NIH), Bethesda, MD, USA).

To measure electrical properties, sintered samples were polished and coated on both sides with gold tincture and fired at 700 °C for 30 min to form electrodes.

Temperature-dependent dielectric permittivity and losses were performed with a precision impedance analyzer Agilent 4294A (Keysight Tech. Inc., Santa Rosa, CA, USA). Complex impedance measures were achieved with an impedance gain/phase analyzer SI 1260 (Solartron Analytical, Hampshire, UK) connected to a dielectric interface 1296 (Solartron Analytical). Experiments were completed using a computer-controlled temperature furnace 47760 (Thermo Fisher Scientific Inc., Waltham, MA, USA) evaluating from 30 °C to 700 °C. The impedance fitting analysis was performed using ZView software (ver. 3.2c Scribner Associates, Inc., Southern Pines, NC, USA).

3. Results and Discussion

3.1. Structural and Microstructural Results

The XRD patterns for BCTZ (x = 0.10, 0.15, 0.18) sintered samples are shown in Figure 1. All compositions exhibited a perovskite-type structure. For x = 0.18, a secondary phase of $CaTiO_3$ was

detected. The XRD patterns indicate that Ca^{2+} and Zr^{4+} ions were incorporated completely into the $BaTiO_3$ lattice (for x = 0.10 and 0.15 compositions) to form a solid solution.

A fine-scanning XRD pattern in the 2θ range of 44°–46° (inset Figure 1) was performed to determine the dependence of the phase structure. A rhombohedral structure with a single (200) peak at 45° was revealed. A further increase in the x content was followed by a pronounced splitting of the (002) peak from the (200) peak, demonstrating a phase transition from rhombohedral to tetragonal phases [14]. The $CaTiO_3$ secondary phase (PDF#042-0423) was detected for x = 0.18. It was speculated that the rhombohedral and tetragonal phases may coexist in the composition range of $0.10 \leq x \leq 0.20$, and consequently, there exists a temperature-independent morphotropic phase boundary (MPB) [15]. The presence of a MPB enhances the electrical performance of BCTZ electroceramics.

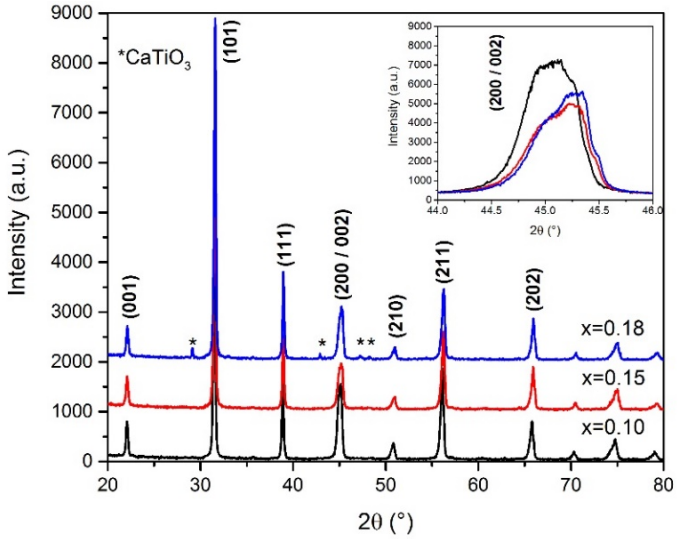

Figure 1. XRD patterns of BCTZ (x = 0.10, 0.15, 0.18) sintered ceramics (1400 °C, 2 h in air). The inset shows a magnification in 2θ between 44° and 46°.

Figure 2a shows the SEM images for sintered pellets at 1400 °C for 2 h with x = 0.10, 0.15 and 0.18. All ceramics revealed a dense microstructure (≈98%). Increasing the Ca^{2+} content at the Ba^{2+} sites decreased the average grain size of the ceramic (22.6, 17.9 and 13.3 μm); moreover, as x = 0.18, the presence of the secondary $CaTiO_3$ phase was promoted due to the proximity of the solubility limit, as revealed by the XRD analysis. Figure 2b shows the EDS spectra for the expected cations of BCTZ and $CaTiO_3$ grains (x = 0.18 sample).

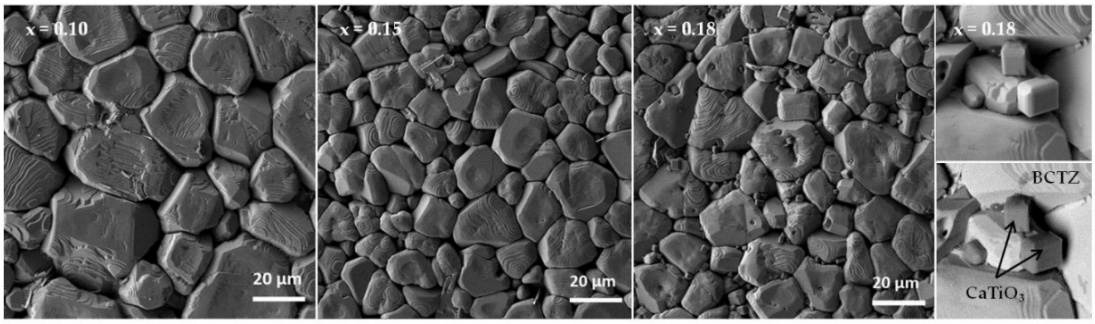

(**a**)

Figure 2. *Cont.*

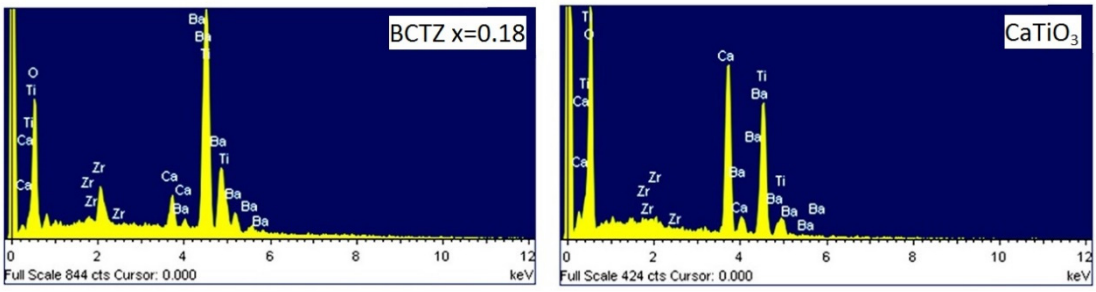

(**b**)

Figure 2. (**a**) SEM micrographs for BCTZ (x = 0.10, 0.15, 0.18) sintered ceramics at 1400 °C for 2 h in air atmosphere; (**b**) EDS spectra of BCTZ and $CaTiO_3$ grains for x = 0.18 sintered ceramic.

3.2. Dielectric Analysis

Dielectric permittivity (ε_r) and losses (*tan* δ) at (1 kHz), as a function of the Ca^{2+} content and temperature, are shown in Figure 3. Two phase transitions corresponding to rhombohedral-tetragonal (*R-T*) and tetragonal-cubic (*T-C*) transitions were observed. The increase of the Ca^{2+} substitution at the Ba^{2+} sites resulted in a displacement, to lower temperatures, of the *R-T* phase transition temperature ($T_{R\text{-}T}$), which was not observable for x = 0.18. The Ca^{2+} addition increases the stability of the temperature range for the tetragonal phase [16]. Furthermore, the dielectric permittivity reached a maximum at x = 0.15, promoted by the MPB. This effect led to a higher number of grains that were favorably oriented towards an electric field, and hence, the optimum piezoelectric and ferroelectric performance could be obtained [1].

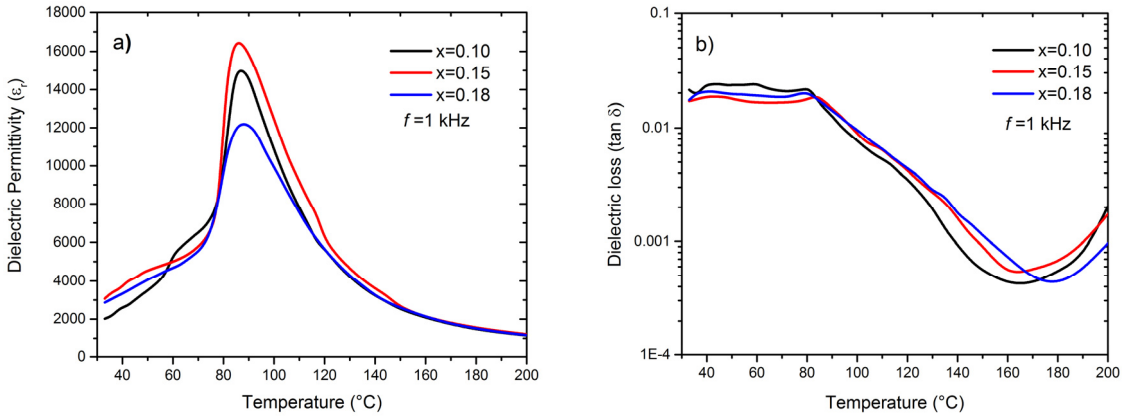

Figure 3. (**a**) Dielectric permittivity and (**b**) losses measured at 1 kHz in BCTZ (x = 0.10, 0.15, 0.18) sintered ceramics (1400 °C; 2 h).

The associated physical properties of BCTZ ceramics after T_C are related to relaxation and conductivity processes [17–21]. For ferroelectric materials, it is important to perform a complete analysis of their electrical properties to separate different electroactive contributions (grain/bulk and grain boundary) and their frequency/temperature dependence. Figure 4b shows a dielectric anomaly (around 400 °C) for $T > T_C$. Temperatures higher than T_C avoid the influence of ferroelectric domains on the ceramic resistance (conduction) because it is well known that defect dipoles and charged species are located at the domain walls [22], which aid the bulk (grain) conduction [11,22].

Despite Ca^{2+} content increases, the dielectric permittivity and losses remained constant for all compositions. Furthermore, Ca^{2+} content shifted the permittivity maxima to lower dielectric values at higher temperatures (around 600 °C). More conveniently seen from the dielectric loss (*tan* δ),

the dielectric anomaly was associated with a process of relaxation [17]: loss peaks shifted toward higher temperatures with an increase in the frequency (Figure 4c).

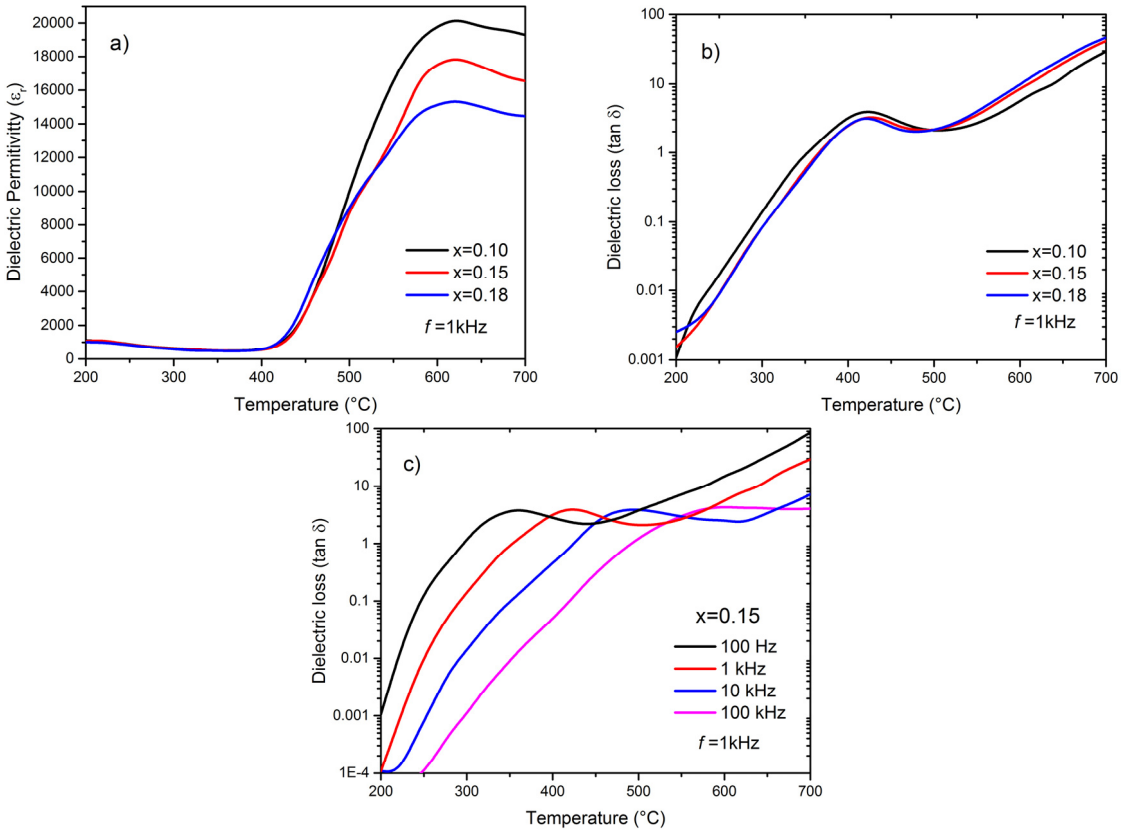

Figure 4. (**a**) Dielectric permittivity and (**b**) losses of BCTZ (x = 0.10, 0.15, 0.18) sintered ceramics (above T_C) at 1 kHz; (**c**) Relaxation process obtained for BCTZ x = 0.15.

For the analysis of BCTZ x = 0.15, wide relaxation peaks were overlapped in a large frequency-dependent range and shifted to higher frequency as the temperature increased. This phenomenon indicates that the dielectric loss peak is related to a thermally activated relaxation process [17]. Moreover, as the Ca^{2+} content increased, the amplitude of the dielectric loss peak decreased, indicating a low activity in the same range of frequencies (Figure 5a–c).

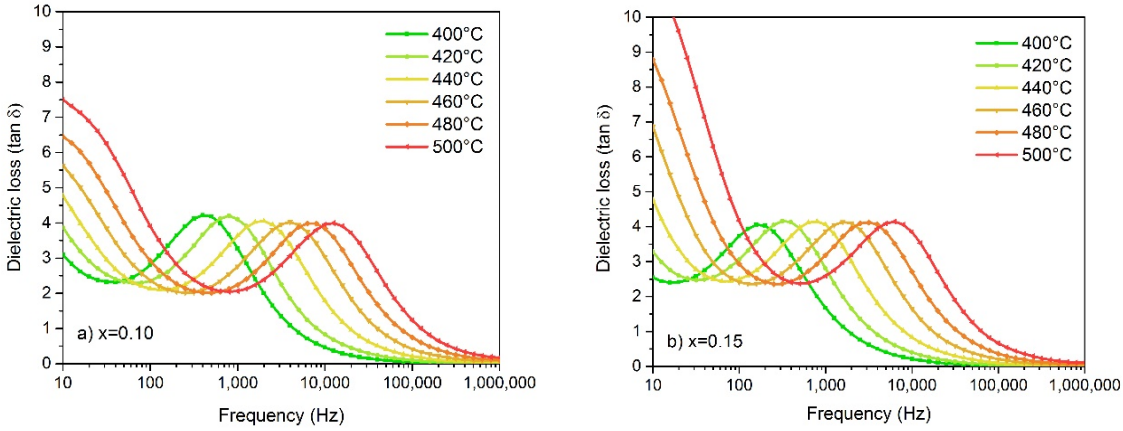

Figure 5. *Cont.*

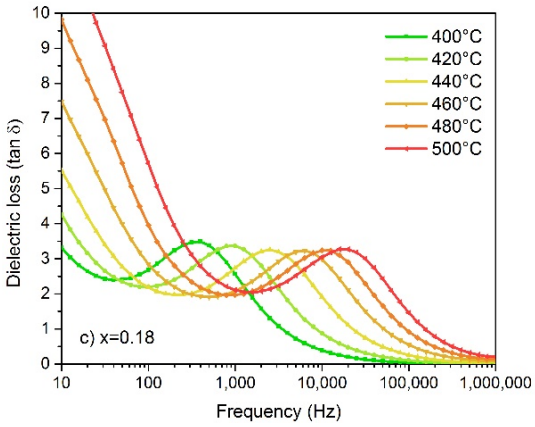

Figure 5. Frequency dependence of dielectric permittivity and dielectric loss for BCTZ (**a**) $x = 0.10$; (**b**) $x = 0.15$; (**c**) $x = 0.18$, measured from 400 °C to 500 °C.

The thermally activated relaxation process follows the Arrhenius law:

$$\tau = \tau_0 \exp\left(Ea/K_B \cdot T\right), \quad (1)$$

where τ_0 is the relaxation time, Ea is the activation energy of the relaxation process, T is the absolute temperature, and K_B is the Boltzmann constant. The resonant condition is $\omega_p \tau_p = 1$, where ω is the angular frequency ($\omega = 2\pi f$) and the subscript p represents the values at the peak maximum position. Figure 6 shows the Arrhenius plots of the dielectric loss peak and the linear fitting for the studied BCTZ compositions. The relaxation parameters obtained from the linear relation, according to Equation (1), are shown in Table 1.

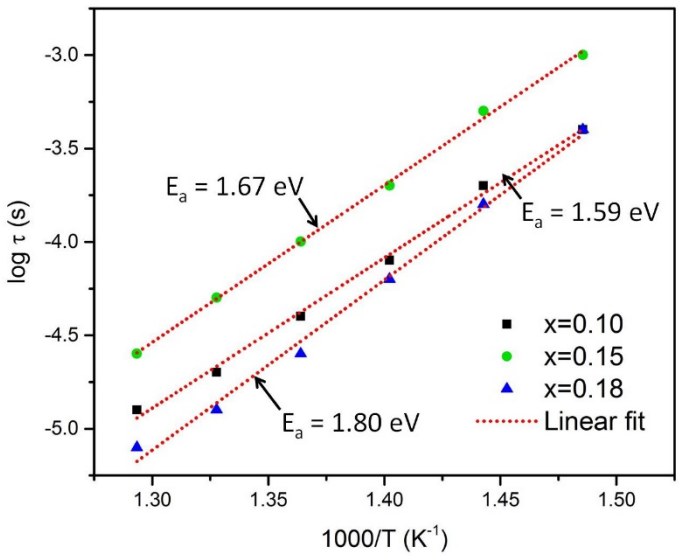

Figure 6. Arrhenius plot of the dielectric relaxation peak from the frequency spectra.

Table 1. Relaxation parameters obtained from the Arrhenius plot.

Composition (x)	τ_0 (s)	Ea (eV)
0.10	4.44×10^{-16}	1.59
0.15	3.42×10^{-16}	1.67
0.18	1.11×10^{-17}	1.80

3.3. Impedance Spectroscopy Analysis

The Nyquist diagrams (Z″ vs. Z′) of BCTZ (x = 0.10, 0.15, 0.18) ceramics, at different temperatures, are shown in Figure 7. The thermal effect over the impedance behavior of the samples became remarkable as temperature increases. Generally used for dielectric materials or ionic conductors, IS is a convenient technique to distinguish between different regions that are responsible for conduction mechanisms [10]. The two semicircles displayed in Figure 7a–c (for sintered BCTZ ceramics at 1400 °C for 2 h) represent the electrical contributions response. From high to low frequency, two semicircles appeared. These phenomena are attributed to the grain/bulk ferroelectric and grain boundary effects, respectively. Semiconducting grains and insulating grain boundaries are characteristic for BCTZ compositions. Moreover, as the radius of the semicircles decreased, the electric resistance dropped.

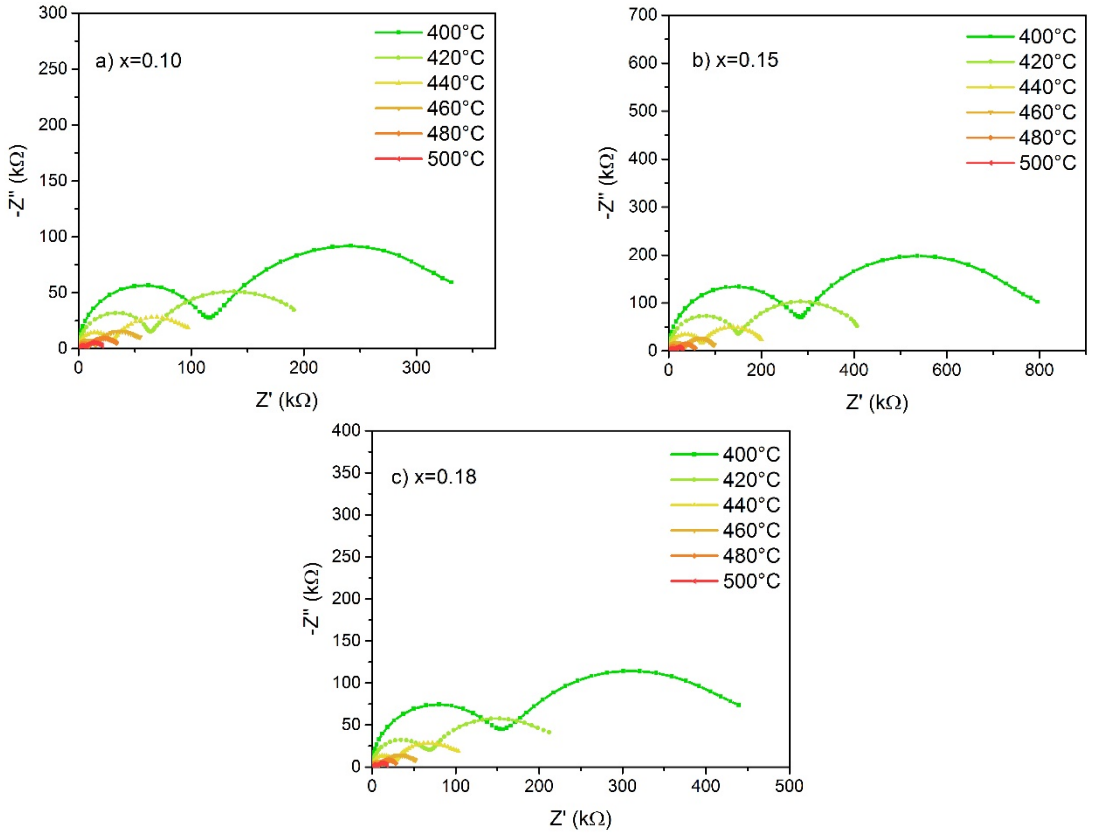

Figure 7. Impedance plots between 400–500 °C for BCTZ (**a**) x = 0.10; (**b**) x = 0.15; (**c**) x = 0.18 compositions sintered at 1400 °C for 2 h.

Increasing the dopant concentration enhances the electronic conductivity until the material reaches a maximum value. The electrical processes, taking place within the material, were modeled for the BCTZ (x = 0.15, 420 °C) system. The electrical properties may be described by an appropriate equivalent circuit, based on a combination of RC (resistor-capacitor) elements in a series and/or parallel arrangement. These RC components represent the macroscopic processes involved in the charge transport due to inhomogeneity over the microstructure. To analyze systems that include a relaxation process, discrete RC elements must be combined with, or replaced by, distributed impedance components. Figure 8 represents the fitting data and the equivalent circuit for BCTZ x = 0.15 at 420 °C. The fitting data (Figure 8a) was done using two R-CPE elements connected in series. The CPE element (constant phase element) was used instead of a pure capacitor to suppress the dispersion and

non-linearities in the values. Then, the values of the resistance (R) and capacitance (C) for the bulk (b) and grain boundary (gb) were calculated. The CPE element is defined as [23,24]:

$$Z_{CPE} = [1/Y_0 (jw)^{\alpha}], \quad (2)$$

where w is the angular frequency, Y_0 is related to the size, thickness and material properties, and α ($0 \leq \alpha \leq 1$) relates to the degree of energy dissipation; it measures the arc depression which is frequency-independent [21]. For $\alpha = 0$, CPE behaves as a resistor. When $\alpha = 1$, CPE behaves as a capacitor. For $\alpha = 0.5$, the CPE element becomes a series RC circuit (Warburg diffusion). The calculated α value of BCTZ $x = 0.15$ is ≈1.

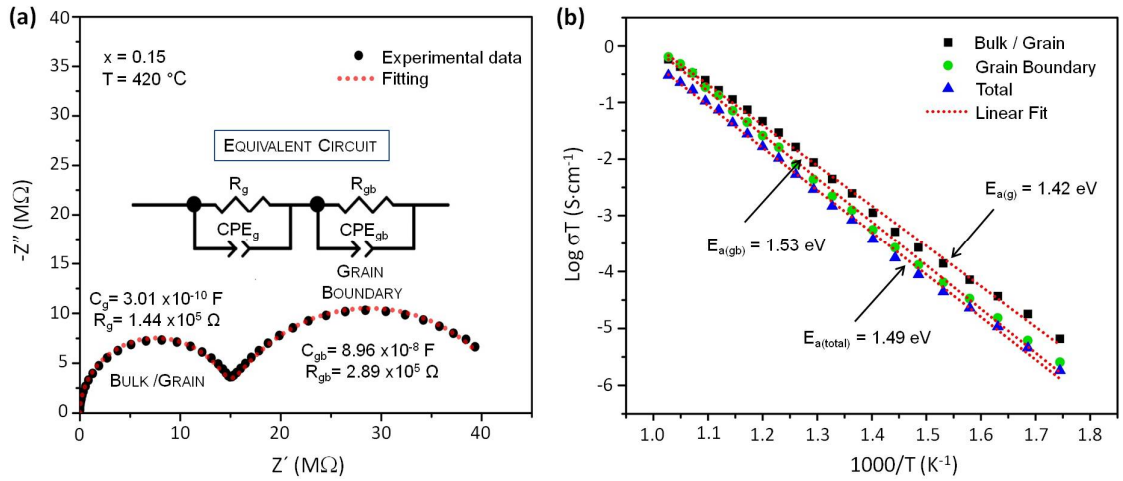

Figure 8. (**a**) Nyquist plot with fitting/simulated equivalent circuit and (**b**) activation energies calculated for the temperature dependence on BCTZ $x = 0.15$.

Associated capacitances led to the identification of different processes: C_g (10^{-9}–10^{-10} F) for bulk/grain ferroelectric ceramics and C_{gb} (10^{-8} F) for the grain boundary. The fitting measured impedances for equivalent circuits elements are: $C_g = 3.01 \times 10^{-10}$ F and $R_g = 1.44 \times 10^5$ Ω; $C_{gb} = 8.96 \times 10^{-8}$ F and $R_{gb} = 2.89 \times 10^5$ Ω, for BCTZ $x = 0.15$ samples measured at 420 °C. These results reveal a well-sintered material with narrow intergranular regions [10].

Like the relaxation time, the electrical conductivity for sintered BCTZ ceramics, measured from 300 °C to 700 °C, follows the Arrhenius law (Equation (1)). Figure 8b shows the activation energy calculated for each region: the bulk/grain, grain boundary and total. The total conductivity response (σ_{total}) is 2.31×10^{-4} S·cm^{-1}, with a bulk conductivity (σ_b) of 7.07×10^{-4} S·cm^{-1} and a grain boundary conductivity (σ_{gb}) of 3.64×10^{-4} S·cm^{-1}. Following the relationship ($\sigma \propto R^{-1}$), the maximum conductivity (σ_{max}) of the material is noticed at the minimum value of the arc response. For the obtained BCTZ $x = 0.15$, $\sigma_{max} = 2.48 \times 10^{-2}$ S·cm^{-1} is reached at 580 °C.

4. Conclusions

BCTZ ceramics were obtained by conventional solid state method. It was found that the studied compositions exhibited a perovskite phase, except for $x = 0.18$ where a secondary phase of $CaTiO_3$ appears. The dielectric permittivity showed a maximum value at $x = 0.15$, promoted by the MPB (i.e., due to higher polarizability promoted by the coexistence of rhombohedral-tetragonal phases). For $T > T_C$, a thermally relaxation process was found. Moreover, EIS analyses showed that conduction phenomena are associated with the bulk and grain boundary regions. For these processes, a suitable equivalent circuit was proposed with R and CPE elements. The maximum conductivity for BCTZ ($x = 0.15$) was found at 580 °C.

Acknowledgments: A Reyes-Montero wants to thank CONACyT-México for providing a PhD scholarship. The authors thanks Federico González García and LDRX-UAMI (T-128) for X-ray diffraction measurements; also Omar Novelo Peralta and Josué Esau Romero Ibarra for SEM image acquisition (IIM-UNAM). María Elena Villafuerte-Castrejón kindly acknowledges PAPIIT-UNAM (IN102715) for financial support. Amador M. González acknowledges the Spanish MEC Project MAT2013-40722-R.

Author Contributions: Armando Reyes-Montero, María Elena Villafuerte-Castrejón and Rigoberto López-Juárez conceived and designed the experiments for the BCTZ synthesis and sintering process. Amador M. González and Paola Ramos-Alvarez performed dielectrical and spectroscopy impedance analyses characterization. Amador M. González revised the obtained electrical data. All authors coordinated in the discussion and writing of the paper.

Conflicts of Interest: The authors declare no conflict of interest.

References

1. Liu, W.; Ren, X. Large piezoelectric effect in Pb-free ceramics. *Phys. Rev. Lett.* **2009**, *103*, 257602. [CrossRef] [PubMed]
2. Bao, H.; Zhou, C.; Xue, D.; Gao, J.; Ren, X. A modified lead-free piezoelectric BZT-xBCT system with higher T_C. *J. Phys D Appl. Phys.* **2012**, *43*, 465401. [CrossRef]
3. Cui, Y.; Liu, X.; Jiang, M.; Zhao, X.; Shan, X.; Li, W.; Yuan, C.; Zhou, C. Lead-free $(Ba_{0.85}Ca_{0.15})(Ti_{0.9}Zr_{0.1})O_3$-$CeO_2$ ceramics with high piezoelectric coefficient obtained by low-temperature sintering. *Ceram. Int.* **2012**, *38*, 4761–4764. [CrossRef]
4. Jiang, M.; Lin, Q.; Lin, D.; Zheng, Q.; Fan, X.; Wu, X.; Sun, H.; Wan, Y.; Wu, L. Effects of MnO_2 and sintering temperature on microstructure, ferroelectric, and piezoelectric properties of $Ba_{0.85}Ca_{0.15}Ti_{0.90}Zr_{0.10}O_3$ lead-free ceramics. *J. Mater. Sci.* **2013**, *48*, 1035–1041. [CrossRef]
5. Tan, C.K.I.; Yao, K.; Ma, J. Effects of LiF on the Structure and Properties of $Ba_{0.85}Ca_{0.15}Zr_{0.1}Ti_{0.9}O_3$ Lead-Free Piezoelectric Ceramics. *Int. J. Appl. Ceram. Technol.* **2013**, *10*, 701–706. [CrossRef]
6. Reyes-Montero, A.; Pardo, L.; López-Juárez, R.; González, A.M.; Cruz, M.P.; Villafuerte-Castrejón, M.E. Lead-free $Ba_{0.9}Ca_{0.1}Ti_{0.9}Zr_{0.1}O_3$ piezoelectric ceramics processed below 1300 °C. *J. Alloys Compd.* **2014**, *584*, 28–33. [CrossRef]
7. Sahoo, G.K.; Mazumder, R. Low temperature synthesis of $Ba(Zr_{0.2}Ti_{0.8})O_3$–$0.5(Ba_{0.7}Ca_{0.3})TiO_3$ nanopowders by solution based auto combustion method. *J. Mater. Sci. Mater. Electron.* **2014**, *25*, 3515–3519. [CrossRef]
8. Chen, L.; Li, L.; Wang, X.; Tian, Z.; Gui, Z. The study of Ca-doped BCTZ ceramics sintered in reducing atmosphere. *J. Electroceram.* **2008**, *21*, 569–572. [CrossRef]
9. Macdonal, J.-R. *Impedance Spectroscopy*; Wiley: Chichester, UK, 1987.
10. Irvine, J.T.S.; Sinclair, D.C.; West, A.R. Electroceramics: Characterization by Impedance Spectroscopy. *Adv. Mater.* **1990**, *2*, 132–138. [CrossRef]
11. West, A.R.; Sinclair, D.C.; Hirose, N. Characterization of Electrical Materials, Especially Ferroelectrics, by Impedance Spectroscopy. *J. Electroceram.* **1997**, *1*, 65–71. [CrossRef]
12. Sinclair, D.C. Characterization of Electro-materials using ac Impedance Spectroscopy. *Bol. Soc. Esp. Cerám. Vidrio* **1995**, *3*, 55–65.
13. Hirose, N.; West, A.R. Impedance Spectroscopy of Undoped $BaTiO_3$ Ceramics. *J. Am. Ceram. Soc.* **1996**, *79*, 1633–1641. [CrossRef]
14. Wu, J.; Xiao, D.; Wu, W.; Chen, Q.; Zhu, J.; Yang, Z.; Wang, J. Composition and poling condition-induced electrical behavior of $(Ba_{0.85}Ca_{0.15})(Ti_{1-x}Zr_x)O_3$ lead-free piezoelectric ceramics. *J. Eur. Ceram. Soc.* **2012**, *32*, 391–398. [CrossRef]
15. Reyes-Montero, A.; Pardo, L.; López-Juárez, R.; González, A.M.; Rea-López, S.O.; Cruz, M.P.; Villafuerte-Castrejón, M.E. Sub-10 μm grain size $Ba_{1-x}Ca_xTi_{0.9}Zr_{0.1}O_3$ (x = 0.10 and x = 0.15) piezoceramics processed using a reduced thermal treatment. *Smart Mater. Struct.* **2015**, *8*, 065033. [CrossRef]
16. Mitsui, T.; Westphal, W.B. Dielectric and x-ray studies of $Ca_xBa_{1-x}TiO_3$ and $Ca_xSr_{1-x}TiO_3$. *Phys. Rev.* **1961**, *124*, 1354–1359. [CrossRef]
17. Tao, J.; Yi, Z.; Liu, Y.; Zhang, M.; Zhai, J. Dielectric Tunability, Dielectric Relaxation, and Impedance Spectroscopic Studies on $(Ba_{0.85}Ca_{0.15})(Ti_{0.9}Zr_{0.1})O_3$ Lead-Free Ceramics. *J. Am Ceram. Soc.* **2013**, *96*, 1847–1851. [CrossRef]

18. Rafiq, M.A.; Rafiq, M.N.; Saravanan, K.V. Dielectric and impedance spectroscopic studies of lead-free barium-calcium-zirconium-titanium oxide ceramics. *Ceram. Int.* **2015**, *41*, 11436–11444. [CrossRef]
19. Wang, X.; Liang, P.; Chao, X.; Yang, Z. Dielectric Properties and Impedance Spectroscopy of $MnCO_3$-Modified $(Ba_{0.85}Ca_{0.15})(Zr_{0.1}Ti_{0.9})O_3$ Lead-Free Ceramics. *J. Am. Ceram. Soc.* **2015**, *98*, 1506–1514. [CrossRef]
20. Liu, Y.; Pu, Y.; Sun, Z.; Jin, Q. Relaxor behavior and complex impedance studies on $Ba_{0.9}Ca_{0.1}Ti_{0.9}Zr_{0.1}O_3$–$0.06Fe^{3+}$ ceramics prepared by hydrothermal method. *J. Mater. Res. Bull.* **2015**, *70*, 195–199. [CrossRef]
21. Sateesh, P.; Omprakash, J.; Kumar, G.S.; Prasad, G. Studies of phase transition and impedance behavior of $Ba(Zr,Ti)O_3$ ceramics. *J. Adv. Dielectr.* **2015**, *5*, 1550002. [CrossRef]
22. Genenko, Y.A.; Glaum, J.; Hoffmann, M.J.; Albe, K. Mechanisms of aging and fatigue in ferroelectrics. *Mater. Sci. Eng. B* **2015**, *192*, 52–82. [CrossRef]
23. Jorcin, J.B.; Orazem, M.E.; Pebere, N.; Tribollet, B. CPE analysis by local electrochemical impedance spectroscopy. *Electrochim. Act.* **2006**, *51*, 1473–1479. [CrossRef]
24. Morrison, F.D.; Jung, D.J.; Scott, J.F. Constant-phase-element (CPE) modeling of ferroelectric random-access memory lead zirconate-titanate (PZT) capacitors. *J. Appl. Phys.* **2007**, *101*, 094112. [CrossRef]